

Parton Distribution Function of a Deuteron-like Dibaryon System from Lattice QCD



Chen Chen,^{1,2} Liuming Liu,^{1,*} Peng Sun,^{1,†} Yi-Bo Yang,^{2,3,4,5,‡}
Yiqi Geng,^{1,6} Fei Yao,^{7,8} Jian-Hui Zhang,^{8,§} and Kuan Zhang^{2,3}

¹*Institute of Modern Physics, Chinese Academy of Sciences, Lanzhou 730000, China*

²*University of Chinese Academy of Sciences, School of Physical Sciences, Beijing 100049, China*

³*CAS Key Laboratory of Theoretical Physics, Institute of Theoretical Physics,
Chinese Academy of Sciences, Beijing 100190, China*

⁴*School of Fundamental Physics and Mathematical Sciences,*

Hangzhou Institute for Advanced Study, UCAS, Hangzhou 310024, China

⁵*International Centre for Theoretical Physics Asia-Pacific, Beijing/Hangzhou, China*

⁶*Nanjing Normal University, Nanjing, Jiangsu 210023, China*

⁷*Center of Advanced Quantum Studies, Department of Physics,
Beijing Normal University, Beijing 100875, China*

⁸*School of Science and Engineering, The Chinese University of Hong Kong, Shenzhen 518172, China*

We report a lattice QCD calculation of the parton distribution function (PDF) of a deuteron-like dibaryon system using large-momentum effective theory. The calculation is done on three Wilson Clover ensembles with a fixed lattice spacing $a = 0.105$ fm and two pion masses. The lattice matrix elements are computed at proton momenta up to 2.46 GeV with the signal of high momentum modes being improved by applying the momentum smearing technique. The state-of-the-art renormalization, matching and extrapolation are then applied to obtain the final result of the light-cone PDF. A comparison between the result of the dibaryon system and the sum of the proton and neutron PDFs is also given.

I. INTRODUCTION

Parton distribution functions (PDFs) are widely applied in high-energy physics. On the one hand, they are necessary inputs for computing cross sections in electron-hadron or hadron-hadron collisions. On the other hand, they contain important information about the intrinsic properties of nucleons and nuclei. To date, the PDFs of single-baryon systems like the proton or neutron have been extensively studied both experimentally and theoretically. In the meantime, the PDFs of multi-baryon systems like the deuteron and ${}^3\text{He}$ have also attracted a lot of attention. Comparing the structure functions between single-baryon and multi-baryon systems reveals important insights into the interaction between baryons within a nucleus. For example, the European Muon Collaboration (EMC) first observed in 1983 that the structure functions of the nucleus differ from the sum of the

structure functions of individual nucleons inside the nucleus [1], which is now known as the “nuclear EMC effect”. It can be characterized by the ratio

$$R(D) = \frac{F_2^D}{F_2^p + F_2^n}, \quad (1)$$

with $F_2(x) = x \sum_i f_i(x) Q_i^2$ at the leading-order, $f_i(x)$ is the PDF of the i th quark flavor. The observation of the EMC effect has opened up new avenues of research in nuclear physics, leading to extensive further study and investigation through many experiments [2–6]. On the theoretical side, substantial efforts have also been made to constrain nucleon-nucleon interactions by calculating basic properties of multi-nucleon systems using the lattice QCD (LQCD) approach [7–31]. Among them, the NPLQCD group has pioneered the calculation of moments of the proton, di-proton and ${}^3\text{He}$ systems [8, 9].

In addition, recent theoretical developments [32–37] have also enabled the direct calculation of the Bjorken x -dependence of PDFs from LQCD. In the past few years, various LQCD calculations for nucleon PDFs have been done [38–49], based on either the large-momentum effective theory (LaMET) [33, 34, 50] or the short-distance ex-

* Corresponding author: liuming@impcas.ac.cn

† Corresponding author: pengsun@impcas.ac.cn

‡ Corresponding author: ybyang@itp.ac.cn

§ Corresponding author: zhangjianhui@cuhk.edu.cn

Ensemble	$a(\text{fm})$	$L^3 \times T$	$m_\pi(\text{MeV})$	$m_\pi L$	$m_{\eta_s}(\text{MeV})$
C32P29	0.105	$32^3 \times 64$	292.9(1.2)	4.9	659.1(1.3)
C24P29	0.105	$24^3 \times 72$	293.1(1.3)	3.7	659.7(1.3)
C24P90	0.105	$24^3 \times 72$	940.7(1.2)	12.0	940.7(1.2)

TABLE I. The simulation setup, including lattice spacing a , lattice size $L^3 \times T$, π mass m_π and η_s mass m_{η_s} .

pansion (pseudo-PDF) approach [37]. Applying such calculations to multi-baryon systems will help further elucidate the origin of nuclear effects.

The deuteron is the simplest multi-baryon bound system. It is composed of a proton and a neutron and has a small binding energy of 2.224644(34) MeV. Such a low binding energy poses a significant challenge for identifying a bound state deuteron through LQCD calculations of two-point correlation functions. However, utilizing three-point correlation functions, such as those employed in the calculation of PDFs, could potentially serve as a useful tool to study nuclear effects, as revealed by the EMC effect.

In this work, we calculate the PDF of a deuteron-like dibaryon system using the LaMET approach. The ultraviolet (UV) divergences are removed by a nonperturbative renormalization in the hybrid scheme [51], which has been widely used in previous studies [43, 52, 53]. While only one single lattice spacing is considered in this work, we perform our calculations on ensembles with two different pion masses at 941 MeV and 293 MeV. To assess the impact of finite volume effects, we conduct simulations at the lower pion mass of 293 MeV on two sets of ensembles with lattice size $32^3 \times 64$ and $24^3 \times 72$. In order to study the nuclear effect, we make a comparison between the PDF of the dibaryon system and the sum of the proton and neutron PDFs.

The rest of the paper is organized as follows. In Sec. II, we describe the calculation of bare matrix elements in lattice simulations. In Sec. III, we outline the procedure of renormalization and matching. In Sec. IV, we present the numerical results of the x -dependent PDF and the ratio of the dibaryon system PDF and the sum of the proton and neutron PDFs. Finally, a summary is given in Sec. V.

II. LATTICE SIMULATION

A. Lattice setup

Throughout the paper, we use the $2 + 1$ flavor QCD ensembles with stout smeared clover fermion action and Symanzik gauge actions generated by the CLQCD collaboration [54, 55]. Three ensembles, named C32P29, C24P29 and C24P90 are used to calculate the bare matrix elements of the nucleon and dibaryon systems. The detailed information is given in Table I.

B. Light-cone PDF v.s. Quasi-PDF

The unpolarized PDF is defined as

$$q(x, \mu) = \int \frac{d\xi^-}{4\pi} e^{-ixP^+\xi^-} \langle P | \bar{\psi}(\xi^-) \gamma^+ U(\xi^-, 0) \psi(0) | P \rangle, \quad (2)$$

where $|P\rangle$ denotes the ground state of a nucleon or a multi-nucleon system with momentum P , x is the momentum fraction carried by the quark, μ is the renormalization scale and $\xi^\pm = (\xi^t \pm \xi^z)/\sqrt{2}$ are light-cone coordinates. The Wilson line along the light-cone direction

$$U(\xi^-, 0) = \mathcal{P} \exp \left[ig \int_0^{\xi^-} du n \cdot A(un) \right] \quad (3)$$

is introduced to ensure gauge invariance of the non-local quark bilinear correlator.

The PDF involves real-time dependence and cannot be directly accessed on the lattice. However, according to LaMET, one can start from the calculation the quasi-PDF, which takes the following form

$$\tilde{q}(x, P_z) = \int \frac{dz}{4\pi} e^{-ixzP_z} \langle P | \bar{\psi}(z) \Gamma U(z, 0) \psi(0) | P \rangle, \quad (4)$$

where the matrix element on the r.h.s. is often called the quasi-light-front (quasi-LF) correlation, P_z representing the momentum of a nucleon or a multi-nucleon system along z -direction. Γ can be chosen as γ_t or γ_z for unpolarized quark quasi-PDFs. In this work, we choose $\Gamma = \gamma_t$, which is free from operator mixing with scalar quark quasi-PDF operator [56–58]. The relation between the quasi-PDF and the light-cone PDF is given by a factorization formula

$$\tilde{q}(x, P_z) = \int_{-1}^1 \frac{dy}{|y|} C \left(\frac{x}{y}, \frac{\mu}{yP_z} \right) q(y, \mu) + \mathcal{O} \left(\frac{\Lambda_{\text{QCD}}^2}{(xP_z)^2}, \frac{\Lambda_{\text{QCD}}^2}{((1-x)P_z)^2} \right), \quad (5)$$

where $q(y, \mu)$ is the light-cone PDF depending on the renormalization scale, $C \left(\frac{x}{y}, \frac{\mu}{yP_z} \right)$ is the matching kernel and $\mathcal{O} \left(\frac{\Lambda_{\text{QCD}}^2}{(xP_z)^2}, \frac{\Lambda_{\text{QCD}}^2}{((1-x)P_z)^2} \right)$ denote higher-twist contributions suppressed by P_z .

C. Two-point and three-point correlators

The momentum-projected two-point correlator $C^{2\text{pt}}(\vec{P}; t_{\text{sep}})$ and three-point correlator $C_\Gamma^{3\text{pt}}(\vec{P}; t, t_{\text{sep}})$ can be defined as

$$C^{2\text{pt}}(\vec{P}; t) = \langle 0 | N_\sigma(\vec{P}; t) N_\sigma^\dagger(\vec{P}; 0) | 0 \rangle, \quad (6)$$

$$C_\Gamma^{3\text{pt}}(\vec{P}; z; t, t_{\text{sep}}) = \langle 0 | N_\sigma(\vec{P}; t_{\text{sep}}) O_\Gamma(z; t) N_\sigma^\dagger(\vec{P}; 0) | 0 \rangle.$$

Here $N_\sigma(\vec{P}, t)$ denotes the nucleon or multi-nucleon interpolating operators projected to certain momentum \vec{P} ; t_{sep} denotes the time interval between the source and the sink with the source being placed at $t = 0$, and σ labels the rows of a certain irreducible representation under which the operator transforms. $O_\Gamma(z; t) = \bar{\psi}(z; t)\Gamma U(z, 0; t)\psi(0; t)$ where $\Gamma = \gamma_t$ is the current operator located at time t with quark and anti-quark separated along the z direction.

We construct the interpolating operators of nucleon and deuteron following the method proposed in Ref. [7]. Since a nucleon has quantum numbers $J^P = \frac{1}{2}^+$, the operator should transform in the G_1^+ irrep of the cubic group. The proton interpolating operator can be written as

$$p_\sigma(\vec{x}; t) = \varepsilon^{abc} u_\zeta^a(\vec{x}; t) (C\gamma_5 P_+)_{\zeta\xi} d_\xi^b(\vec{x}; t) \times (P_+)_{\sigma\rho} u_\rho^c(\vec{x}; t), \quad (7)$$

where C is the charge conjugation matrix and P_+ is the positive-parity projection operator $P_+ = \frac{1+\gamma_4}{2}$. Note that the gamma matrices here are in Dirac-Pauli representation and $\sigma \in \{0, 1\}$. Neutron operator $n_\sigma(\vec{x}; t)$ can be obtained by swapping u and d in Eq. (7).

In order to efficiently compute the Wick contractions of the correlation functions, one can rewrite the nucleon interpolating operators above as the following [7]:

$$p_\sigma(\vec{x}; t) = \sum_\alpha w_\alpha^{[N]\sigma} u^{i(\alpha)}(\vec{x}; t) d^{j(\alpha)}(\vec{x}; t) u^{k(\alpha)}(\vec{x}; t),$$

$$n_\sigma(\vec{x}; t) = \sum_\alpha w_\alpha^{[N]\sigma} d^{i(\alpha)}(\vec{x}; t) u^{j(\alpha)}(\vec{x}; t) d^{k(\alpha)}(\vec{x}; t), \quad (8)$$

where quark fields are labeled with indices i, j, k, \dots , which are a combination of spinor and color indices. For example, $i = (\zeta, a)$ with spinor index $\zeta \in \{0, 1, 2, 3\}$ and color index $a \in \{0, 1, 2\}$; $w_\alpha^{[N]\sigma}$ denotes the weights of different spin-color combination, with $\alpha \in \{1, \dots, \mathcal{N}_w^{[N]}\}$ running over the $\mathcal{N}_w^{[N]}$ combinations of $u^{i(\alpha)} d^{j(\alpha)} u^{k(\alpha)}$. For each σ , only 12 terms appear due to the sparseness of gamma matrices and antisymmetric tensor ε^{abc} , which significantly reduces the computation time for contractions.

Nucleon operators making up momentum-projected correlators in Eq. (6) can be obtained by the Fourier transform

$$p_\sigma(\vec{P}; t) = \sum_{\vec{x} \in \Lambda} e^{i\vec{P}\cdot\vec{x}} p_\sigma(\vec{x}; t),$$

$$n_\sigma(\vec{P}; t) = \sum_{\vec{x} \in \Lambda} e^{i\vec{P}\cdot\vec{x}} n_\sigma(\vec{x}; t). \quad (9)$$

In our calculation $\vec{P} = (0, 0, (2\pi n)/L)$ is directed along the z -axis. In principle, the operators should be summed over all spatial lattice sites for both the sink and the source. However, this approach would necessitate the calculation of all-to-all propagators, which is infeasible

given our limited computational resources. As a practical compromise, we sum over all spatial lattice sites for the sink and a few points evenly distributed in the $z = 0$ plane for the source. Specifically, we contract point-to-all propagators with sources fixed at one point, enhance the measurements by shifting the source position, and repeat the calculation. This method is also applied to the calculation of deuteron-like dibaryon correlators.

Deuteron has quantum numbers $I(J^P) = 0(1^+)$. Therefore, we build the following two-nucleon interpolating operators:

$$D_1(\vec{P}; t) = \sum_{\vec{x}_1, \vec{x}_2 \in \Lambda} e^{i\frac{\vec{P}}{2}\cdot(\vec{x}_1+\vec{x}_2)} \frac{1}{\sqrt{2}} [p_0(\vec{x}_1; t)n_0(\vec{x}_2; t) - n_0(\vec{x}_1; t)p_0(\vec{x}_2; t)],$$

$$D_2(\vec{P}; t) = \sum_{\vec{x}_1, \vec{x}_2 \in \Lambda} e^{i\frac{\vec{P}}{2}\cdot(\vec{x}_1+\vec{x}_2)} \frac{1}{2} [p_0(\vec{x}_1; t)n_1(\vec{x}_2; t) + p_1(\vec{x}_1; t)n_0(\vec{x}_2; t) - n_0(\vec{x}_1; t)p_1(\vec{x}_2; t) - n_1(\vec{x}_1; t)p_0(\vec{x}_2; t)],$$

$$D_3(\vec{P}; t) = \sum_{\vec{x}_1, \vec{x}_2 \in \Lambda} e^{i\frac{\vec{P}}{2}\cdot(\vec{x}_1+\vec{x}_2)} \frac{1}{\sqrt{2}} [p_1(\vec{x}_1; t)n_1(\vec{x}_2; t) - n_1(\vec{x}_1; t)p_1(\vec{x}_2; t)], \quad (10)$$

where the subscripts of $D_{\{1,2,3\}}$ represent the three components of $J = 1$, and \vec{P} is the center of mass momentum of the system. For simplicity we only consider the case in which both the proton and the neutron carry half of the total momentum. \vec{x}_1 and \vec{x}_2 are space coordinates of the two nucleons. These operators are used at the sink, while at the source the two nucleons are put at the same space position since we compute point-to-all quark propagators as explained above.

The quark-level representation of dibaryon operators can be constructed by inserting Eq. (8) into Eq. (10):

$$D_\rho(\vec{P}; t) = \sum_{\vec{x}_1, \vec{x}_2 \in \Lambda} e^{i\frac{\vec{P}}{2}\cdot(\vec{x}_1+\vec{x}_2)} \sum_\alpha w_\alpha^{[D]\rho} u_g^{i(\alpha)}(\vec{x}_1, t) d_g^{j(\alpha)}(\vec{x}_1, t) u_g^{k(\alpha)}(\vec{x}_1, t) \times d_g^{l(\alpha)}(\vec{x}_2, t) u_g^{m(\alpha)}(\vec{x}_2, t) d_g^{n(\alpha)}(\vec{x}_2, t). \quad (11)$$

where the weights $w_\alpha^{[D]\rho}$, with $\alpha \in \{1, \dots, \mathcal{N}_w^{[D]\rho}\}$, with $\mathcal{N}_w^{[D]1} = \mathcal{N}_w^{[D]3} = 144$ and $\mathcal{N}_w^{[D]2} = 288$, are obtained from products of weights of nucleon $w_\alpha^{[N]\sigma}$ as shown in [7].

The three-point correlation function can be obtained by summing over all possible contractions of connected diagrams. Our calculation did not account for the disconnected diagram contributions, which are not expected to have a significant impact our qualitative findings [59]. In

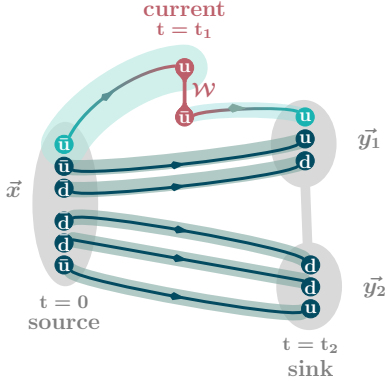


FIG. 1. Illustration of the three-point correlator of a deuteron-like system before momentum projection (one possible way of contraction).

Ensemble	$P_z^{nucleon}$ (GeV)	t_{sep}/a	N_{conf}	$nsrc$ (time \times space)
C32P29	1.48	6,7,8	870	4×4
	1.85	6,7,8		4×4
	2.21	6,7,8		4×4
C24P29	1.48	6,7,8	759	3×2
	1.97	6,7,8		3×8
	2.46	6,7,8		6×8
C24P90	1.48	6,7,8,9,10	750	3×1
	1.97	6,7,8,9		3×1
	2.46	6,7,8		3×4

TABLE II. Information on nucleon's momentum $P_z^{nucleon}$ (the center-of-mass momentum of dibaryon system is $2P_z^{nucleon}$), time separation between source and sink (t_{sep}) and number of sources ($nsrc$) on the $z = 0$ plane used to calculate two-point and three-point correlators.

Fig. 1 we give an illustration of one possible contraction of the three-point correlator of the deuteron-like dibaryon system.

Three ensembles, namely C32P29, C24P29 and C24P90, are used to calculate two-point and three-point correlators of the deuteron-like dibaryon system and the nucleon. The calculations are performed with the nucleon carrying different momenta $P_z^{nucleon} = (2\pi n)/L$ along the z -direction and the total momentum of the dibaryon system is $2P_z^{nucleon}$. For each momentum, several sets of source-sink separations t_{sep} are calculated. For larger momenta, correlators are averaged over several sources evenly distributed on the $z = 0$ plane to control the statistical uncertainties. The detailed information is shown in Table II.

To improve the signal of high momentum states, we applied momentum-Gaussian smearing on sources and sinks [60], which takes the form

$$\begin{aligned} \psi(x) &\rightarrow S_{mom}\psi(x) \\ &= (1 - \alpha)\psi(x) + \frac{\alpha}{6} \sum_j U_j(x) e^{ik\hat{e}_j} \psi(x + \hat{e}_j) \\ &= (1 + \frac{\alpha}{6} a^2 D_j D_j) \psi(x) + \mathcal{O}(a^3), \end{aligned} \quad (12)$$

where k represents the momentum-smearing parameter, U_j denotes a stout-smear gauge link along a specified direction. The above operation should be iterated by $n_{iter} = \mathcal{O}(2\sigma^2)$ times to achieve the desired smearing size σa , which corresponds to $n_{iter} = 50$ and $\sigma a = 0.5$ fm in our calculation. This process shifts the smearing center to momentum $\mathcal{O}(k)$, thereby significantly improving the signal of high-momentum states. In our calculation we set k equals to half of the nucleon momentum, which is the optimized choice to improve the signal according to previous experience. In addition, we applied one-step hypercubic(HYP)-smearing on the Wilson link of the current operator.

D. Joint fitting

The two-point correlator (2pt) $C^{2pt}(P_z, t)$ and three-point correlator (3pt) $C_\Gamma^{3pt}(P_z, t, t_{sep})$ can be decomposed as

$$\begin{aligned} C^{2pt}(P_z; t) &= |\mathcal{A}_0|^2 e^{-E_0 t} + |\mathcal{A}_1|^2 e^{-E_1 t} + \dots, \\ C_\Gamma^{3pt}(P_z; z; t, t_{sep}) &= |\mathcal{A}_0|^2 \langle 0 | \mathcal{O}_\Gamma(z; t) | 0 \rangle e^{-E_0 t_{sep}} \\ &\quad + |\mathcal{A}_1|^2 \langle 1 | \mathcal{O}_\Gamma(z; t) | 1 \rangle e^{-E_1 t_{sep}} \\ &\quad + \mathcal{A}_1 \mathcal{A}_0^* \langle 1 | \mathcal{O}_\Gamma(z; t) | 0 \rangle e^{-E_1(t_{sep}-t)} e^{-E_0 t} \\ &\quad + \mathcal{A}_0 \mathcal{A}_1^* \langle 0 | \mathcal{O}_\Gamma(z; t) | 1 \rangle e^{-E_0(t_{sep}-t)} e^{-E_1 t} + \dots, \end{aligned} \quad (13)$$

where $\langle 0 | \mathcal{O}_\Gamma | 0 \rangle$ is the desired ground-state quasi-matrix elements; $|n\rangle$ with $n > 0$ represents the excited states; $\mathcal{A}_{0,1}$ are amplitudes depending on smearing parameters; $E_{0,1}$ are the ground state and excited state energy, respectively; and the ellipse denotes the contribution from $n > 1$ excited states which decays faster than the ground and first excited states. P_z is the momentum along z direction.

The above expressions can be further simplified into the fitting form

$$\begin{aligned} C^{2pt}(P_z, t) &\approx c_4 e^{-E_0 t} (1 + c_5 e^{-\Delta E t}), \\ R_\Gamma^{3pt}(P_z, t, t_{sep}) &\equiv \frac{C_\Gamma^{3pt}(t, t_{sep})}{C^{2pt}(t_{sep})}, \\ &\approx \frac{c_0 + c_1 e^{-\Delta E(t_{sep}-t)} + c_2 e^{-\Delta E t} + c_3 e^{-\Delta E t_{sep}}}{1 + c_5 e^{-\Delta E t_{sep}}}, \end{aligned} \quad (14)$$

Ensemble	c_2	c_3	$\chi^2/d.o.f.$
C32P29	1.067(29)	-0.022(50)	1.43
C24P29	1.085(28)	-0.015(19)	0.33
C24P90	0.953(14)	-0.0054(99)	0.81

TABLE III. Fitting result of dispersion relation $E(p)^2 = E_0^2 + c_2 p^2 + c_3 p^4 a^2$, including c_2 , c_3 and $\chi^2/d.o.f.$.

where c_0 corresponds to the bare quasi-matrix elements, $\Delta E = E_1 - E_0$ denotes the energy gap between the ground state and the first excited state.

The ground state effective energy E_0 is obtained by fitting the 2pt function in Eq. (14). After obtaining the ground state effective energy $E_0(P_z)$ under different momenta, we fit for the dispersion relation

$$E_0(P_z)^2 = m^2 + c_2 P_z^2 + c_3 P_z^4 a^2. \quad (15)$$

The quadratic term with lattice spacing a is included to parameterize the discretization effects. The fitting results of each ensemble are shown in Fig. 2. The result of c_2 and c_3 is shown in Table III.

To obtain bare matrix elements c_0 , we apply the joint fit of 2pt and the ratio of 3pt to 2pt at several t_{sep} s. For the ensembles C24P29 and C32P29, the fit range of 2pt starts from $t = 2a$ while for the ensemble C24P90, the excited states decay faster, and the fit range starts from $t = 1a$. The correlators are Jackknife resampled before fitting. For each t_{sep} of the ratio, we choose the fit range as $t \in [1, t_{sep} - 1]$ to eliminate the contribution of higher excited states.

For the nucleon case, the source and sink are symmetric, allowing us to set $c_1 = c_2$. However, for the dibaryon system, the correlator consists of a hexaquark source and a dibaryon sink, so we treat c_1 and c_2 as two independent variables. Given the significant correlation between the 2pt and the ratio, we combine the data of the 2pt and the ratio into one correlation matrix in the fitting. In Fig. 3, we plot the ratio of 3pt to 2pt, taking the largest momentum case of the dibaryon system as an example. Fitting results of other momenta and for the nucleon are shown in Appendix VI A. The ground state contribution c_0 obtained by the fit is shown as the gray band. Our fitting results are compared with the original data, demonstrating that the data for each t_{sep} can be well described by the fit.

III. RENORMALIZATION AND MATCHING

A. Hybrid renormalization

The bare quasi-LF correlation can be multiplicatively renormalized as

$$\tilde{h}(z, P_z, 1/a) = Z_L(a) e^{-\delta m(a)z} \tilde{h}_R(z, P_z, 1/a), \quad (16)$$

Ensemble	a (fm)	$L^3 \times T$	m_π (MeV)	$m_\pi L$	m_{η_s} (MeV)
C32P29	0.105	$32^3 \times 64$	292.9(1.2)	4.9	659.1(1.3)
H48P32	0.0519	$48^3 \times 144$	319.0(1.7)	4.0	695.6(3.5)
F32P30	0.0775	$32^3 \times 96$	303.6(1.3)	3.8	677.67(90)

TABLE IV. The lattice setup for simulating zero-momentum pion hadron matrix elements.

where $\tilde{h}_R(z, P_z, 1/a)$ is the renormalized quasi-LF correlation, $Z_L(a)$ contains all z-independent logarithmic UV divergences, $\delta m(a)$ includes the z-dependent linear UV divergences from Wilson-line self-energy. To remove these divergences, some non-perturbative renormalization approaches have been proposed and implemented in the literature [61–66]. However, they suffer from the fact that the renormalization factor contains undesired non-perturbative contributions, which distort the IR behavior of the original quasi-LF correlation. In our work, we adopt the so-called hybrid renormalization to avoid this problem [51]. More precisely, we renormalize the quasi-LF correlations at short and long distances differently. At short distances, the renormalization is carried out by dividing by the same hadron matrix element in the rest frame, as is done in the ratio scheme [64]. At long distances, the renormalized factor for quasi-LF correlations is determined by the self-renormalization [67] by fitting the bare matrix elements at multiple lattice spacings to a parametrization formula containing discretization effects and linear divergences. The renormalized quasi-LF correlation then takes the following form:

$$\begin{aligned} \tilde{h}_R(z, P_z) = & \frac{\tilde{h}(z, P_z, 1/a)}{\tilde{h}(z, P_z = 0, 1/a)} \theta(z_s - |z|) \\ & + \eta_s \frac{\tilde{h}(z, P_z, 1/a)}{Z_R(z, 1/a)} \theta(|z| - z_s), \end{aligned} \quad (17)$$

where z_s is introduced to divide the short and long distances, and $Z_R(z, 1/a)$ indicates the renormalization factor extracted from the self-renormalization procedure, which includes the linear divergence part $\delta m(a)$ and some discretization effects. The scheme conversion factor η_s is to ensure the continuity of the renormalized quasi-LF correlation at $z = z_s$.

Since the renormalization follows from the UV property of the quark bilinear operator, we can choose the pion hadron matrix element in the rest frame to extract the renormalization factor. The corresponding lattice setup is shown in Table IV. We start from the normalized pion matrix elements in the rest frame

$$\tilde{h}_B^\pi(z, P_z = 0, 1/a) = Z_R(z, 1/a) \tilde{h}_R^\pi(z, P_z = 0) \quad (18)$$

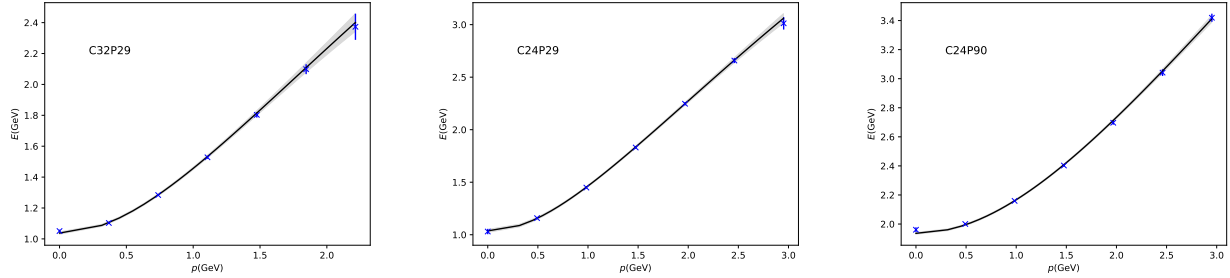


FIG. 2. The dispersion relation $E_0(P_z)^2 = m^2 + c_2 P_z^2 + c_3 P_z^4 a^2$ of each ensemble used in this work.

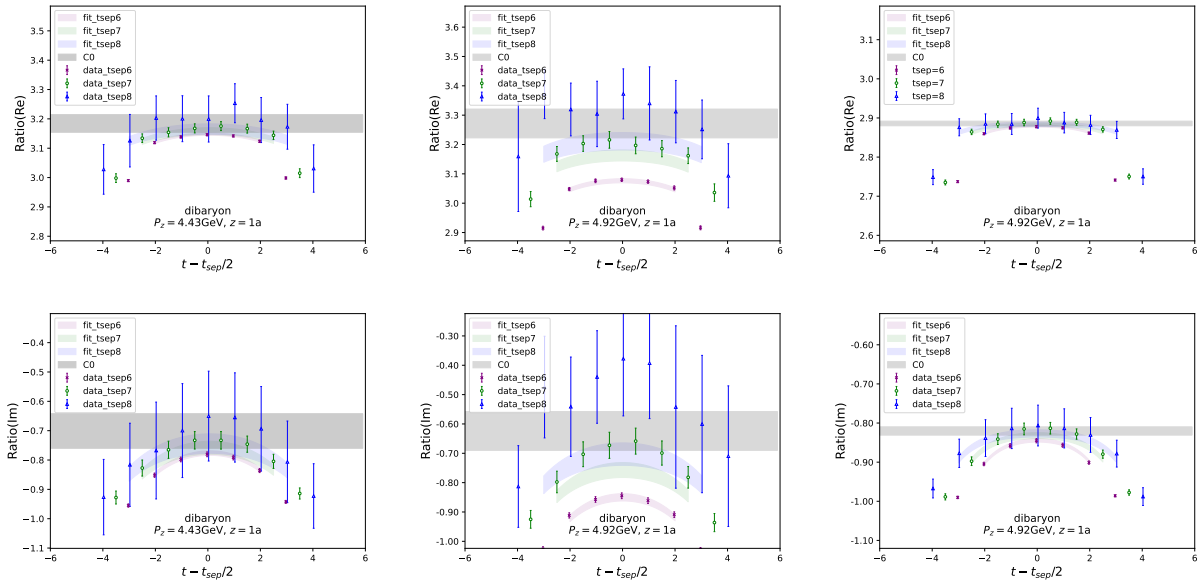


FIG. 3. Demonstration of fitting the correlation function on each ensemble C32P29(left), C24P29(middle) and C24P90(right). Here we present the $z = 1a$ dibaryon result of the largest momentum case of each ensemble as an example. We compare the lattice data of the ratio (error bars) and results predicted by the fitting (colored bands). The ground state contribution c_0 obtained by the fitting is shown as the gray band.

with

$$Z_R(z, 1/a) = \exp \left\{ \frac{kz}{a \ln[a\Lambda_{\text{QCD}}]} + m_0 z + f(z) a^2 + \frac{3C_F}{b_0} \ln \left[\frac{\ln[1/(a\Lambda_{\text{QCD}})]}{\ln[\mu/\Lambda_{\text{QCD}}]} \right] + \frac{1}{2} \ln \left[1 + \frac{d}{\ln[a\Lambda_{\text{QCD}}]} \right]^2 \right\}, \quad (19)$$

where the first term on the r.h.s. is the linear divergence, and $m_0 z$ denotes a finite mass contribution from the renormalization ambiguity. $f(z) a^2$ represents the discretization effects and the last two terms come from the resummation of leading and sub-leading logarithmic divergences. According to Ref. [67], the fitting parameters k and $f(z)$ are related to the specific lattice action, while d and m_0 are determined by matching to the continuum scheme at short distances. In the $\overline{\text{MS}}$ scheme, the short distance result takes the following form at the next-to-

leading order (NLO)[62]

$$C_{0,\text{NLO}}(z, \mu) = 1 + \frac{\alpha_s C_F}{4\pi} \left(3 \ln \frac{z^2 \mu^2}{4e^{-2\gamma_E}} + 5 \right). \quad (20)$$

In our calculation, we choose to determine the parameters in Z_R through a global fit as follows

$$\begin{aligned} \ln \tilde{h}_B^\pi(z, P_z = 0, 1/a) &= \frac{kz}{a \ln[a\Lambda_{\text{QCD}}]} + f(z) a^2 \\ &+ \frac{3C_F}{b_0} \ln \left[\frac{\ln(1/a\Lambda_{\text{QCD}})}{\ln(\mu/\Lambda_{\text{QCD}})} \right] + \frac{1}{2} \ln \left[1 + \frac{d}{\ln[a\Lambda_{\text{QCD}}]} \right]^2 \\ &+ \begin{cases} \ln[C_{0,\text{NLO}}(z, \mu)] + m_0 z & \text{if } z_0 \leq z \leq z_1 \\ g(z) & \text{if } z_1 < z \end{cases}, \quad (21) \end{aligned}$$

where k , Λ_{QCD} , $f(z)$, m_0 , d and $g(z)$ are treated as free fitting parameters. We choose $z_0 = 0.05$ fm, $z_1 = 0.2$ fm and the maximum value of z is 1.55 fm.

parameter	fit result
k	0.674(0.008)
$\Lambda_{\text{QCD}}(\text{GeV})$	0.16(0.03)
$m_0(\text{GeV})$	0.14(0.06)
d	-0.04(0.02)
$\chi^2/d.o.f.$	1.03

TABLE V. The parameters and $\chi^2/d.o.f.$ are determined by doing a global fit for Eq. (21).

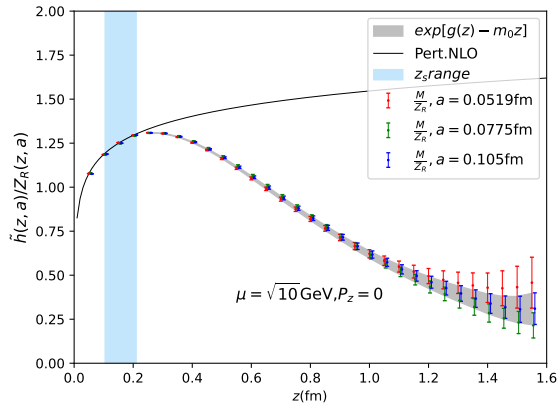


FIG. 4. Comparison of renormalized matrix elements with the perturbative one-loop $\overline{\text{MS}}$ results (black curve). Error bars represents the renormalized matrix elements of each lattice spacing. $g(z)$ is the residual from the fitting process [67] and $\text{Exp}[g(z) - m_0 z]$ (gray band) indicates the a -independent renormalized matrix element. z_s (introduced to divide short and long distance in hybrid scheme) is taken as 0.21 fm and varied down to 0.105 fm to estimate systematic uncertainties, as shown by the blue band.

According to Ref. [67], to account for additional systematic uncertainties related to $a\mu$, the input error of uncorrelated fit can be modified as

$$(\sigma_{\ln \bar{h}})_{\text{new}} = \sqrt{(\sigma_{\ln \bar{h}})_{\text{old}}^2 + (\delta_{\text{sys}} a \mu)^2},$$

where δ_{sys} is set to be 0.0005. By doing this more weights can be given to the small lattice spacing data during the fitting process. The fitting results of parameters and the $\chi^2/d.o.f.$ are shown in Table V.

The comparison of the renormalized matrix element with the perturbative one-loop $\overline{\text{MS}}$ result is given in

Fig. 4. This figure shows a good agreement between the renormalized matrix element and the continuum one-loop result at short distances, except at very small z , where higher-order corrections become important. In this way, we take $z_s = 0.21$ fm in the hybrid renormalization process and vary it down to 0.105 fm to estimate the systematic uncertainty related to the choice of z_s .

As a function of z , the renormalized matrix elements are plotted in Fig. 5. We present the results of the dibaryon system and of free nucleons (proton and neutron) simultaneously. As shown in the figure, the results exhibits a convergence trend with increasing P_z for different ensembles. For larger momentum, statistical uncertainties are controlled by increasing the number of sources in space.

B. Large- λ extrapolation and Fourier transform

As can be seen from the figures of renormalized matrix elements, the uncertainties become worse with increasing $\lambda = zP_z$. However, a Fourier transform to momentum space requires the quasi-correlator at all distances. To resolve this issue, we follow [51] and adopt an extrapolation with the following form in the large λ region

$$\tilde{h}_R(\lambda) = \left[\frac{c_1}{(i\lambda)^a} + e^{-i\lambda} \frac{c_2}{(-i\lambda)^b} \right] e^{-\lambda/\lambda_0}, \quad (22)$$

where the algebraic terms in the square bracket are associated with a power law behavior of the unpolarized PDFs in the endpoint region, and the exponential term comes from the expectation that at finite momentum the correlation function has a finite correlation length (denoted as λ_0) [51], which becomes infinite with the momentum approaching infinity. In Fig. 6, we show the extrapolation result of the dibaryon system with $P_z = 2.95$ GeV for the ensemble C32P29. After the λ extrapolation, we can perform a Fourier transform and obtain the x -dependent quasi-PDF in momentum space.

C. Matching and infinite momentum extrapolation

As mentioned before, we neglect the contribution of disconnected diagrams and mixing with gluons. Therefore, the dibaryon and nucleon PDFs can be extracted through a perturbative matching shown in Eq. (5), where the corresponding perturbative kernel up to the NLO in the hybrid scheme reads [68, 69]

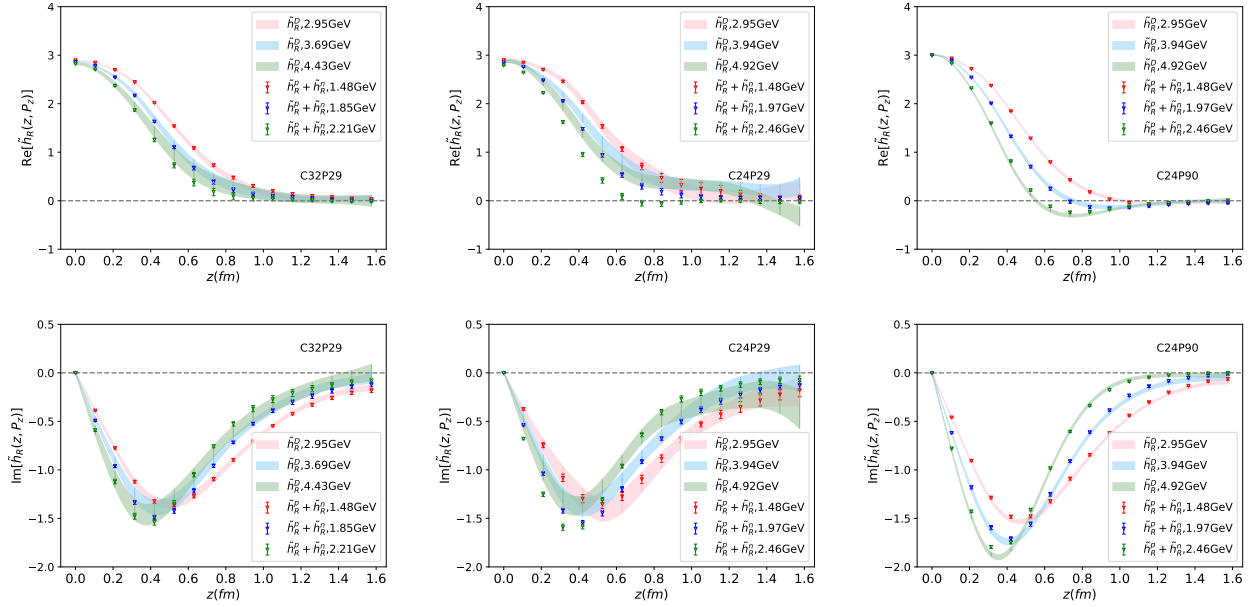


FIG. 5. The real and imaginary part of renormalized matrix elements of C32P29 (left) , C24P29 (middle) and C24P90(right) as a function of z at scale $\mu = \sqrt{10}$ GeV. Different color represents different momentum of external state. The colored bands and error bars represent the renormalized matrix elements for a dibaryon and for the sum of a proton and a neutron, respectively.

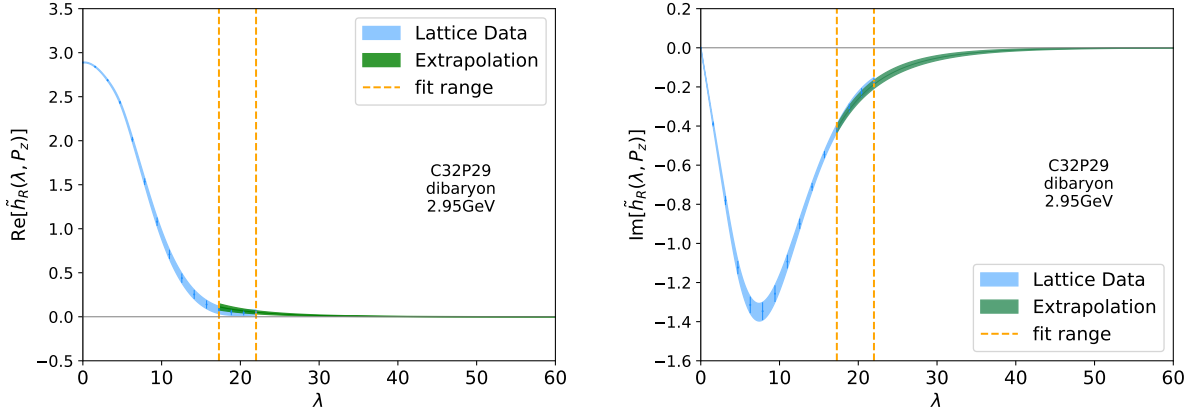


FIG. 6. The large- λ extrapolation of renormalized matrix elements for the case of a dibaryon system with $P_z = 2.95$ GeV for ensemble C32P29. The blue and green bands represent lattice data and extrapolated results respectively. The orange dashed lines mark off the fit range for Eq. 22. As can be seen from the plot, our fitting results agree well with lattice data within the fit range.

$$C_{\text{ratio}}\left(\xi, \frac{\mu}{yP_z}\right) = \delta(1-\xi) + \frac{\alpha_s C_F}{2\pi} \begin{cases} \left[\frac{1+\xi^2}{1-\xi} \ln \frac{\xi}{\xi-1} + 1 - \frac{3}{2(1-\xi)} \right]_+ & \xi > 1 \\ \left[\frac{1+\xi^2}{1-\xi} \left(-\ln \frac{\mu^2}{y^2 P_z^2} + \ln 4\xi(1-\xi) - 1 \right) + 1 + \frac{3}{2(1-\xi)} \right]_+ & 0 < \xi < 1 \\ \left[-\frac{1+\xi^2}{1-\xi} \ln \frac{\xi}{\xi-1} - 1 + \frac{3}{2(1-\xi)} \right]_+ & \xi < 0, \end{cases} \quad (23)$$

$$C_{\text{hybrid}}(\xi, \lambda_s, \frac{\mu}{yP_z}) = C_{\text{ratio}}\left(\xi, \frac{\mu}{yP_z}\right) + \frac{3\alpha_s C_F}{4\pi} \left(\frac{1}{|1-\xi|} + \frac{2\text{Si}((1-\xi)|y|\lambda_s)}{\pi(1-\xi)} \right)_+, \quad (24)$$

with $\xi = \frac{x}{y}$

We also need to extrapolate to infinite momentum to extract the physical unpolarized PDF. Here we use the following ansatz which takes into account the leading power contribution

$$q_0(x, \mu, P_z) = q(x, \mu) + \frac{d_0}{(P_z)^2}, \quad (25)$$

where $q_0(x, \mu, P_z)$ on the l.h.s. denotes the PDF results obtained under different momenta, and $q(x, \mu)$ is the physical PDF in the infinite momentum limit.

IV. NUMERICAL RESULTS

In Fig. 7, we show an estimate of systematic and statistical uncertainties of the light-cone PDF, taking the dibaryon result on the ensemble C32P29 as an example. The systematic uncertainties mainly have four sources. The first is the λ extrapolation. We take the difference between the results with two fit ranges, $\{P_z = 2.95 \text{ GeV} : \lambda \geq 11aP_z, P_z = 3.69 \text{ GeV} : \lambda \geq 11aP_z, P_z = 4.43 \text{ GeV} : \lambda \geq 11aP_z\}$ and $\{P_z = 2.95 \text{ GeV} : \lambda \geq 9aP_z, P_z = 3.69 \text{ GeV} : \lambda \geq 10aP_z, P_z = 4.43 \text{ GeV} : \lambda \geq 10aP_z\}$ as an estimate of the systematic uncertainty due to the λ extrapolation. The second is the renormalization scale dependence, estimated by varying the scale from $\sqrt{10} \text{ GeV}$ to 2 GeV and taking their difference. The third is the uncertainty from momentum extrapolation and we take the difference between results extrapolated to infinite momentum and that given by largest momentum as an estimation. The last contribution is from the choice of z_s in the hybrid scheme. The error is estimated by calculating the difference between the results at $z_s = 0.21 \text{ fm}$ and $z_s = 0.105 \text{ fm}$.

By comparing the difference between the PDFs of the multi-baryon system and the sum of a proton and a neutron, we can obtain information about the interaction between the baryons inside a nucleus. However, the difference in the definitions of momentum fraction x makes it difficult to do the comparison directly. For a free nucleon the momentum fraction is defined as $x = \frac{p}{P_z^{nucleon}}$, where p and $P_z^{nucleon}$ represent the longitudinal momenta of the parton and the nucleon, respectively. For a multi-nucleon system with each of the N nucleons carrying the same momentum, the momentum fraction is defined as $x' = \frac{p}{NP_z^{nucleon}}$. Therefore, before doing the comparison, we have to rescale the PDF of a multi-nucleon system. Given that $x = Nx'$, the PDF after rescaling $q^{rescale}(x)$ can be related by the previous one $q(x')$ by

$$q^{rescale}(x) = Cq(x') = Cq\left(\frac{x}{N}\right) \quad (26)$$

where C is a normalization factor. From that

$$\int xq^{rescale}(x)dx = N \int x'q(x')dx', \quad (27)$$

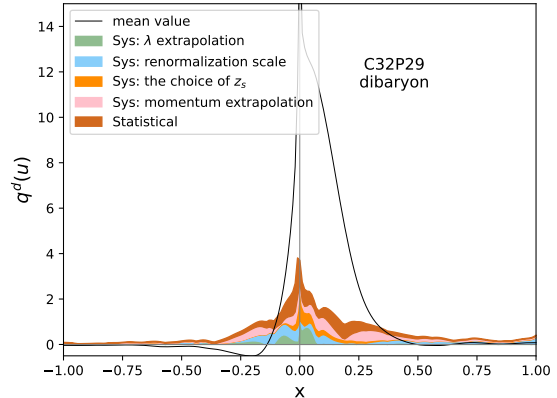


FIG. 7. Estimation of statistical and systematic uncertainties, taking the dibaryon result of the ensemble C32P29 as an example. The width of the (non-overlapping) coloured bands denotes the size of each uncertainty (these uncertainties are added in quadrature and the square root is taken to obtain the full uncertainty), and the black curve is the mean value obtained at $z_s = 0.21 \text{ fm}$, $\mu = \sqrt{10} \text{ GeV}$ and λ extrapolation range $\{P_z = 2.95 \text{ GeV} : \lambda \geq 11aP_z, P_z = 3.69 \text{ GeV} : \lambda \geq 11aP_z, P_z = 4.43 \text{ GeV} : \lambda \geq 11aP_z\}$.

which means that the average momentum fraction after rescaling is N times that before rescaling, we conclude $C = \frac{1}{N}$.

For the PDF of a deuteron-like dibaryon system $q^d(x)$, we have

$$q^{d,rescale}(x) = \frac{1}{2}q^d\left(\frac{x}{2}\right). \quad (28)$$

In Fig. 8 we give an example of the dibaryon PDF before and after rescaling. For a deuteron-like dibaryon system with nucleon-nucleon interaction, the upper limit of x can be 2 after rescaling. The contribution in the region $1 < x < 2$ is from nuclear effects. In Fig. 9, we obtain a clear signal for the dibaryon PDF in the region of $0 < x < 1$. However, in the region of $x > 1$ the dibaryon PDF is zero within uncertainty.

In Fig. 9 we also show the comparison of the rescaled dibaryon PDF and the sum of proton and neutron PDFs, where the uncertainties include both statistical and systematic uncertainties. The light gray bands and shaded deep gray bands denote the regions where LaMET results are not reliable for dibaryon and nucleon respectively, as revealed by the leading infrared renormalon(LRR) [70] and renormalization group resummation(RGR) [71] analysis in Appendix B. Since at small x regions the LRR+RGR-improved results blows up, indicating that higher twist contribution cannot be neglected. Similarly, at large x regions, the same instability occurs. In reliable regions the NLO results are consistent with those incorporating the LRR and RGR effects. For illustration purpose, in Fig. 10 we plot the ratio of the rescaled dibaryon PDF and the sum of proton and neutron PDFs, with x

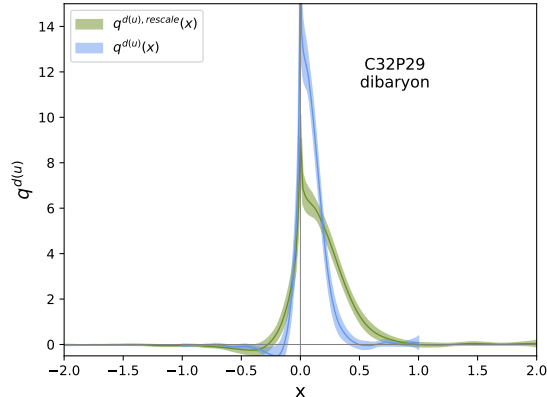


FIG. 8. An example of the deuteron-like dibaryon PDF before (blue band) and after rescaling (green band), taking the result of ensemble C32P29 as an example.

ranging from 0.2 to 0.8 where LaMET theory is reliable. When x is larger than 0.7 divergence appears since nucleon results as denominators are very close to zero. One can see that at $m_\pi \sim 293$ MeV, the dibaryon PDF is generally smaller than the sum of proton and neutron PDFs, which is consistent with experiments. The difference is more prominent for the small volume (C24P29) than for the large one (C32P29). At $m_\pi \sim 940$ MeV, the dibaryon PDF is larger than the sum of proton and neutron PDFs. This may indicate different binding nature of the two-nucleon system at different pion masses. Nevertheless, the ratio is consistent with 1 within $1 - 2\sigma$ for all three ensembles. More precise results are required in future studies to provide reliable information on the nuclear effects in the deuteron.

V. SUMMARY

In this paper, We present the first lattice QCD calculation of the quark PDF of the deuteron-like dibaryon system via LaMET method. Our calculation is done on ensembles with a single lattice spacing. With high statistics, we have used multiple source-sink separations to control the excited-state contamination, and applied the state-of-the-art renormalization, matching and extrapolation procedure. We have also studied the momentum dependence, and extrapolated to the infinite momentum limit. For the lattice with a small spatial volume, we find that the PDF exhibits a noticeable difference between the dibaryon system and the sum of a proton and a neutron. As the spatial volume becomes larger, this difference becomes indistinguishable within the current uncertainty.

Clearly, our study requires improvements in various aspects. For example, the current analysis is limited to a single lattice spacing of 0.105fm, with pion masses of the

ensembles at 293 MeV and 940 MeV, which are away from the physical point. To assess these systematic uncertainties, a comprehensive analysis using several ensembles with different lattice spacings and pion masses would be essential, which requires a considerable amount of computing resources. Nevertheless, in this work we study, for the first time, the PDFs of a multi-nucleon system. Our final results demonstrate the potential to detect nuclear effects by investigating PDFs through the LQCD approach.

ACKNOWLEDGMENT

We thank the CLQCD collaborations for providing us with their gauge configurations with dynamical fermions [54], which are generated on HPC Cluster of ITP-CAS, the Southern Nuclear Science Computing Center(SNSC), the Siyuan-1 cluster supported by the Center for High Performance Computing at Shanghai Jiao Tong University and the Dongjiang Yuan Intelligent Computing Center. We are grateful to Ying Chen for the valuable discussion and comments. We thank Wei Wang for his constructive feedback on our work. We would like to thank Xiaonu Xiong for providing us a template for plotting the three-point correlator. We would also like to thank Yushan Su for providing the Mathematica notebook to confirm the correct implementation of RGR and LRR. The calculations were performed using the Chroma software suite [72] with QUDA [73–75] through HIP programming model [76] and software QCU. The numerical calculations in this paper have been carried out the Dongjiang Yuan Intelligent Computing Center, the HPC Cluster of ITP-CAS and the Southern Nuclear Science Computing Center(SNSC). L. Liu is supported in part by National Natural Science Foundation of China (NSFC) under Grant No. 12293061 and 12175279, the Strategic Priority Research Program of the Chinese Academy of Sciences with Grant No. XDB34030301, Guangdong Major Project of Basic and Applied Basic Research No. 2020B0301030008. Y. Yang is supported in part by NSFC under Grants No. 12293062, 12293061, 12293065 and 12047503, and also the education integration young faculty project of University of Chinese Academy of Sciences, the Strategic Priority Research Program of Chinese Academy of Sciences, Grant No. XDB34030303. L. Liu and Y. Yang are supported in part by NSFC under Grants No. 12293060. P. Sun and Y. Yang are supported by Chinese Academy of Sciences under Grant No. YSBR-101. F. Yao and J. H. Zhang are supported in part by National Natural Science Foundation of China under grants No. 12375080, 11975051, and by CUHK-Shenzhen under grant No. UDF01002851. Y. Yang, P. Sun and J. H. Zhang are also supported in part by a NSFC-DFG joint grant under grant No. 12061131006 and SCHA 458/22 and the GHfund A No. 202107011598.

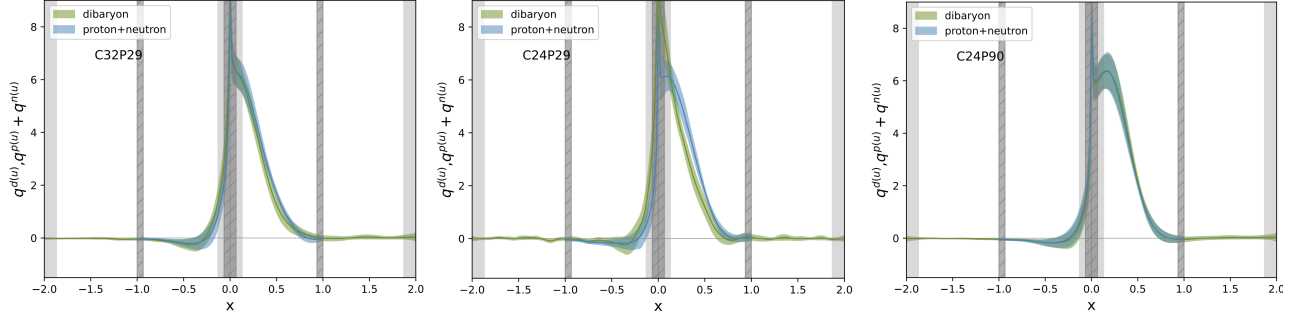


FIG. 9. Our final results on the light-cone PDF at renormalization scale $\mu = \sqrt{10}$ GeV, extrapolated to the infinite momentum limit. The result of the dibaryon (blue bands) and the sum of proton and neutron (green bands) are both plotted for comparison purposes. The light gray bands ($-2 < x < -1.87$, $-0.13 < x < 0.13$, and $1.87 < x < 2$) and shaded deep gray bands ($-1 < x < -0.935$, $-0.065 < x < 0.065$, and $0.935 < x < 1$) denote the regions where LaMET results are considered unreliable for the dibaryon and nucleon, respectively. Since when $-0.13 < x < 0.13$ the LRR+RGR-improved results of dibaryon blows up, indicating that higher twist contributions cannot be neglected. Similarly, at large x regions, the same instability occurs.

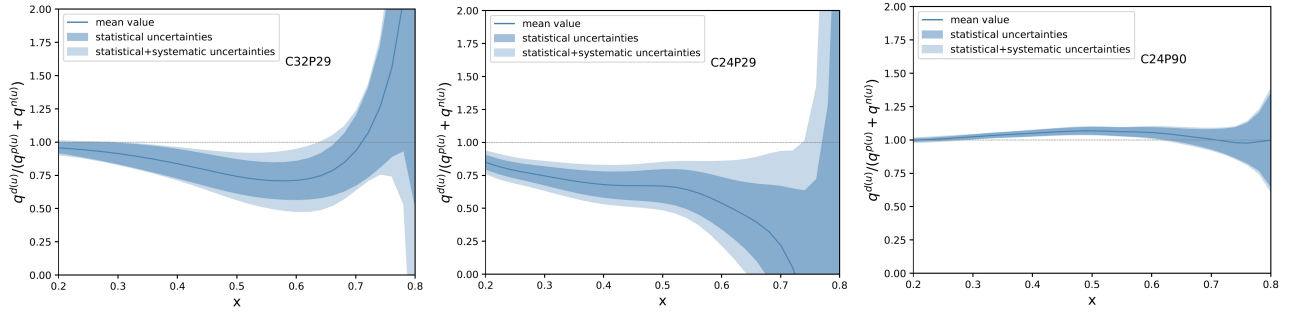


FIG. 10. The ratio of the deuteron-like dibaryon PDF to the sum of proton and neutron PDFs, with x ranging from 0.2 to 0.8 where LaMET theory is reliable. The deep blue bands indicate statistical uncertainties, while the light blue bands represent the combined effects of both statistical and systematic uncertainties. When x is larger than 0.7 divergences appear since nucleon results as denominators are very close to zero.

VI. APPENDIX

A. Details on data analysis

In Fig. 11, Fig. 12 and Fig. 13 we plotted the ratio of 3pt to 2pt, comparing the fitting results with original data. $z = 1a$ results of dibaryon, proton and neutron under different momentum are illustrated in the plots.

In Fig. 14 we present the value of $\chi^2/\text{d.o.f}$ (d.o.f represents degrees of freedom) of correlated fits for c_0 . We take the largest momentum result of dibaryon system depending on different z as an example. Most of the $\chi^2/\text{d.o.f}$ are beneath 1.5 which illustrates the high quality of the fits.

B. Renormalization group resummation and leading renormalon resummation

To determine the scheme-dependence m_0 , the method is the comparison between the renormalized matrix elements and the fixed order Wilson coefficient shown in Eq. (20) at a short distance. In principle, we can resum the large logarithmic terms $\alpha_s^n(\mu)\ln^n(z^2\mu^2)$ in $C_{0,\text{NLO}}$ to reduce the scale dependence. Then the fitting parameters m_0 introduce small deviations from the fixed-order process, changing the z -dependence. Here, the well-known leading infrared renormalon (IRR) arises from the long-distance contributions to the self-energy of the Wilson line, and the asymptotic series is $C(\alpha_s) = \sum_i c_i \alpha_s^i$. The divergence behavior for c_i is the same as the quark ‘‘pole’’ mass $m = \sum_n r_n \alpha_s^{n+1}$ that is well investigated [77]. Therefore, the strategy for IRR here is considering LRR proposed in Ref. [70] by using state-of-the-art knowledge on the mass renormalon,

$$r_n(z, \mu) = N_m |z\mu| \left(\frac{\beta_0}{2\pi} \right)^n \frac{\Gamma(n+1+b)}{\Gamma(1+b)} \times \left(1 + \frac{b}{n+b} c_1 + \frac{b(b-1)}{(n+b)(n+b-1)} c_2 + \dots \right) \quad (29)$$

where the parameters b , c_1 , c_2 and N_m are given in Ref. [70]. One can obtain the leading renormalon contribution through a Borel transformation.

$$C_{0,\text{LRR}}^{\text{PV}}(z, \mu) = N_m |z\mu| \frac{4\pi}{\beta_0} \int_{0,\text{PV}}^{\infty} du e^{-\frac{4\pi u}{\alpha_s(\mu)\beta_0}} \times \frac{1}{(1-2u)^{1+b}} (1 + c_1(1-2u) + c_2(1-2u)^2 + \dots) \quad (30)$$

In practice, the modified Wilson coefficient in the continuum scheme is

$$C_{0,\text{LRR}}(z, \mu) = C_{0,\text{NLO}}(z, \mu) + [C_{0,\text{LRR}}^{\text{PV}}(z, \mu) - \alpha_s(\mu)r_0(z, \mu)]. \quad (31)$$

where the last term $\alpha_s(\mu)r_0(z, \mu)$ is the NLO expansion of $C_{0,\text{LRR}}^{\text{PV}}(z, \mu)$. Now the result contains the fixed-order contribution and the higher-order leading renormalon contribution. In this work, we resum the leading divergent contributions to all orders at $\mu = z^{-1}$ performing RGR [71].

In this way, the m_0 determined using Eq. (30) are shown in Fig. 15 as a function of z . The main values are obtained at $\mu = \sqrt{10}$ GeV by doing global fit. Both statistical and systematic uncertainties are taken into account. The statistical uncertainties remain relatively consistent, regardless of whether LRR and RGR are included. The systematic uncertainties are estimated by varying μ to 2 and 4 GeV. As illustrated in the figure, including the leading renormalon reduces the scale dependence of m_0 . By including LRR and RGR, we improve twist-three power accuracy and high order correction for describing the matrix element in the rest frame, further enhancing the accuracy of the renormalization factor extraction.

In our process, after the renormalization and Fourier transformation, we can extract the unpolarized PDF by applying perturbative matching. It is worth noting that we should add the term ΔC_{LRR} provided in Ref. [70] to the matching kernel C_{hybrid} for LRR correction, and also perform the RGR to reduce the scale dependence as done in Ref. [71].

In Fig. 16, we present the light-cone PDF of dibaryon system after applying LRR and RGR, with only statistical uncertainties taken into consideration. As can be seen from the figure, the LRR+RGR-improved unpolarized PDF blows up in the small x region, indicating that LaMET is unreliable in this region. In reliable region the NLO+LGR+RGR result shows good agreement with fixed-order matching.

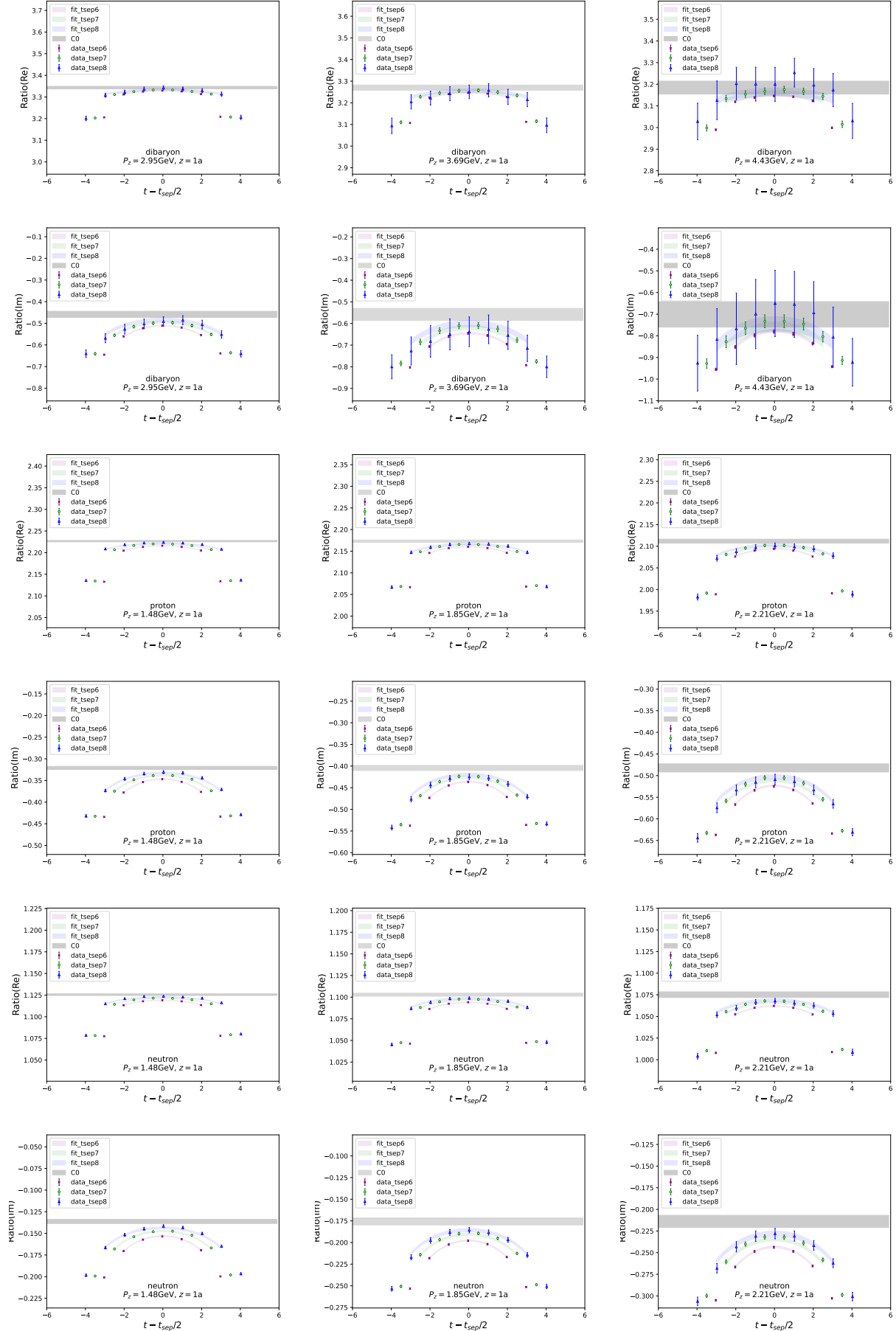


FIG. 11. Demonstration of fitting the correlation function of ensemble C32P29. Here we represent the result of $z = 1a$ of different momentum. We compare the lattice data of ratio (error bars) and results predicted by fitting (colored bands). The ground state contribution c_0 obtained by the fitting is shown as the black band.

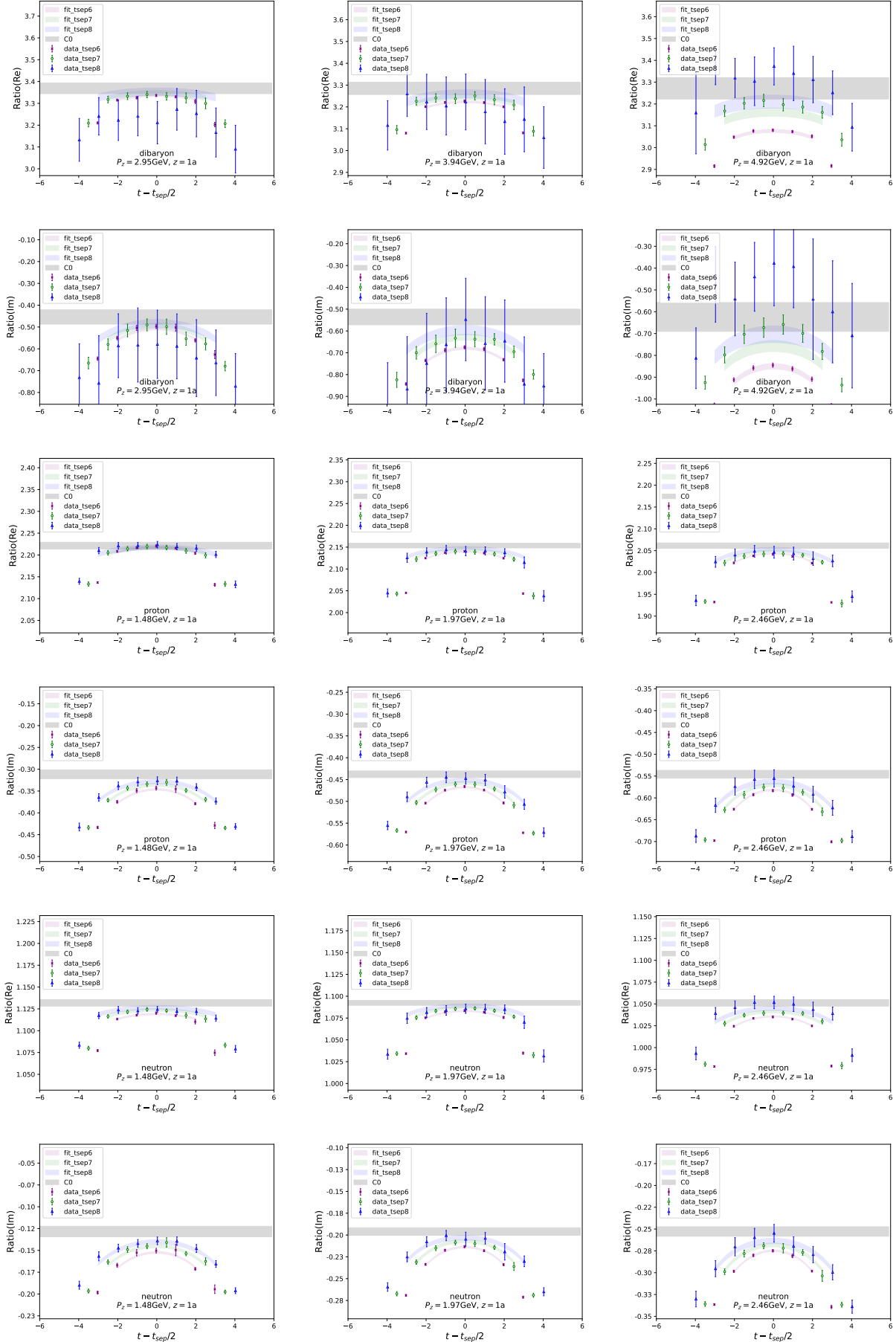


FIG. 12. Demonstration of fitting the correlation function of ensemble C24P29. Here we represent the result of $z = 1a$ of different momentum.

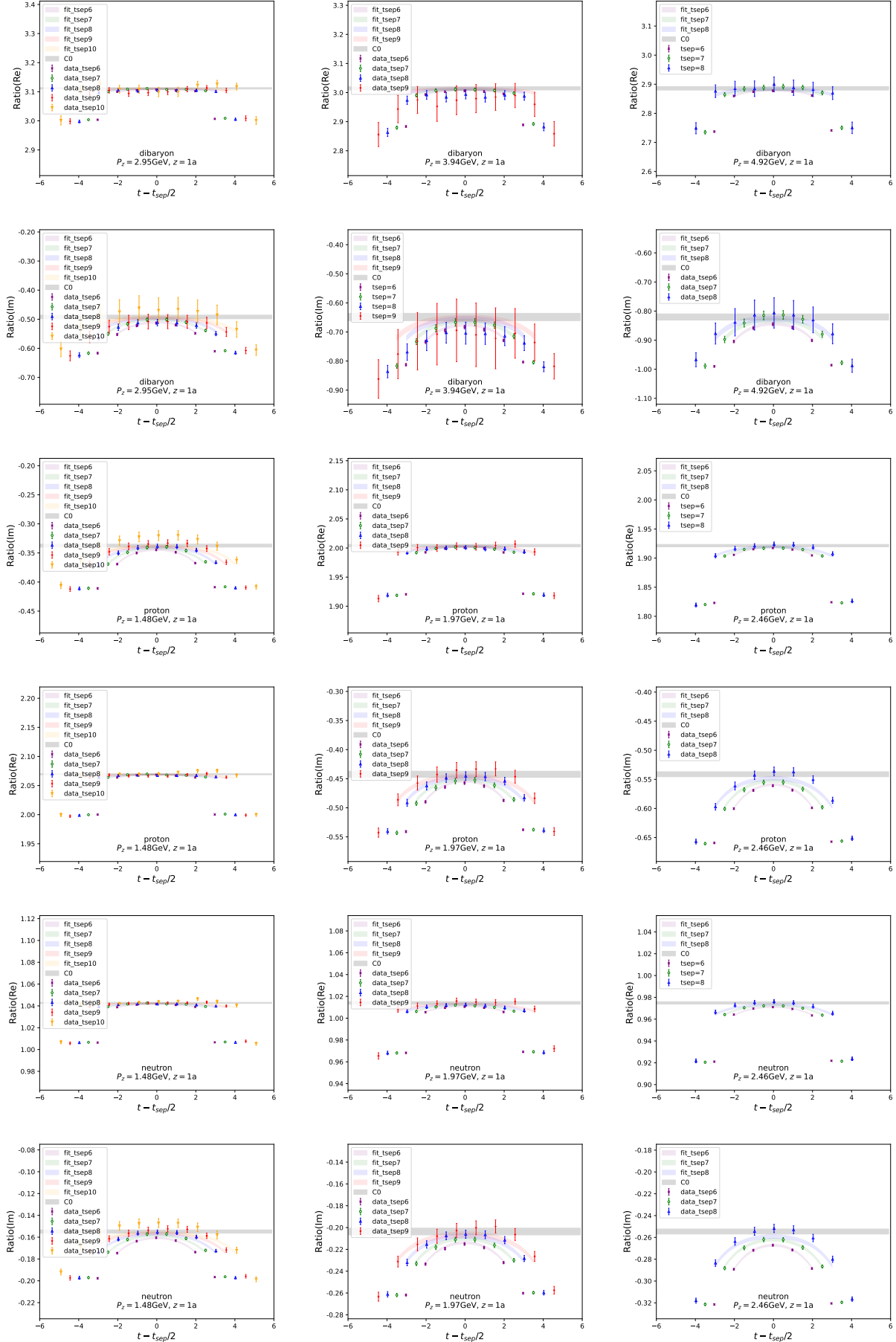


FIG. 13. Demonstration of fitting the correlation function of ensemble C24P90. Here we represent the result of $z = 1a$ of different momentum.

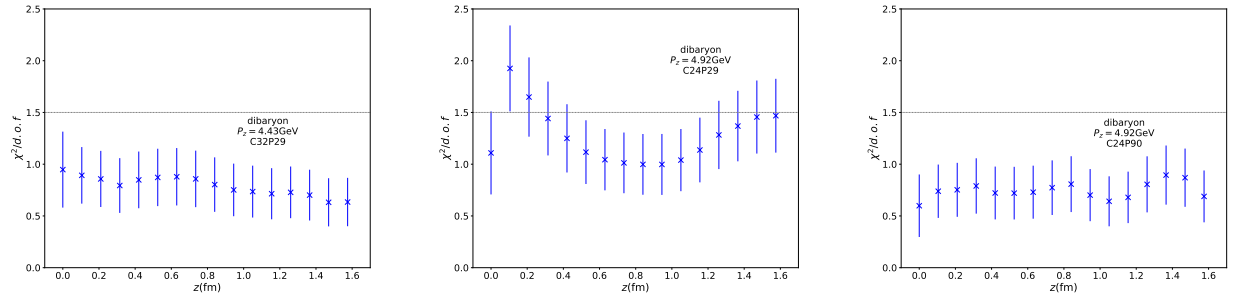


FIG. 14. $\chi^2/\text{d.o.f}$ of correlated fits for c_0 , taking the largest momentum of dibaryon system for each ensemble as an example.

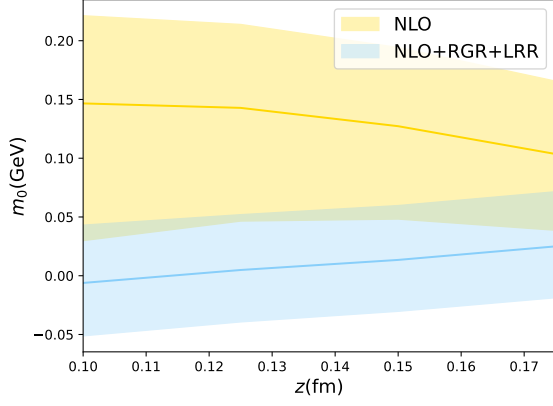


FIG. 15. m_0 determined by using fixed order (NLO) and modified (NLO+LRR+RGR) Wilson coefficient as a function of z . The main values are obtained at $\mu = \sqrt{10}$ GeV. The bands contain both statistical and systematic uncertainties with the latter determined by varying μ to 2 and 4 GeV.

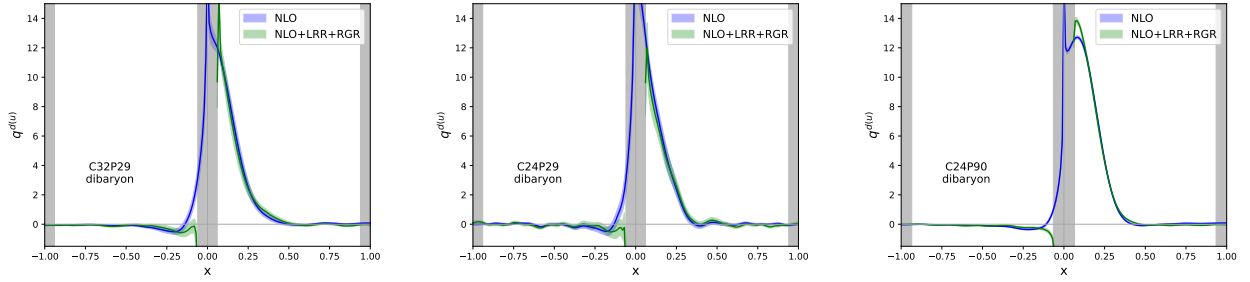


FIG. 16. Comparison between fixed-order matching results of dibaryon PDF (blue bands) and that incorporating the LRR+RGR (green bands). The LRR+RGR results blow up at small x region ($-0.065 < x < 0.065$), indicating that LaMET is unreliable at this region. Only statistical uncertainties are considered in the plots.

-
- [1] J. J. Aubert et al. (European Muon), *Phys. Lett. B* **123**, 275 (1983).
- [2] J. Ashman, B. Badelek, G. Baum, J. Beaufays, C. Bee, C. Benchouk, I. Bird, S. Brown, M. Caputo, H. Cheung, et al., *Physics Letters B* **202**, 603 (1988).
- [3] A. Bodek, N. Giokaris, W. B. Atwood, D. H. Coward, D. J. Sherden, D. L. Dubin, J. E. Elias, J. I. Friedman, H. W. Kendall, J. S. Poucher, et al., *Phys. Rev. Lett.* **50**, 1431 (1983).
- [4] A. Accardi, L. T. Brady, W. Melnitchouk, J. F. Owens, and N. Sato, *Phys. Rev. D* **93**, 114017 (2016), 1602.03154.
- [5] C. Cocuzza, C. E. Keppel, H. Liu, W. Melnitchouk, A. Metz, N. Sato, and A. W. Thomas (Jefferson Lab Angular Momentum (JAM)), *Phys. Rev. Lett.* **127**, 242001 (2021), 2104.06946.
- [6] E. P. Segarra et al., *Phys. Rev. D* **103**, 114015 (2021), 2012.11566.
- [7] S. Amarasinghe, R. Baghdadi, Z. Davoudi, W. Detmold, M. Illa, A. Parreno, A. V. Pochinsky, P. E. Shanahan, and M. L. Wagman, *Phys. Rev. D* **107**, 094508 (2023), 2108.10835.
- [8] W. Detmold, M. Illa, D. J. Murphy, P. Oare, K. Orginos, P. E. Shanahan, M. L. Wagman, and F. Winter (NPLQCD), *Phys. Rev. Lett.* **126**, 202001 (2021), 2009.05522.
- [9] M. Illa (NPLQCD), *PoS LATTICE2021*, 378 (2022), 2112.14226.
- [10] S. R. Beane, P. F. Bedaque, K. Orginos, and M. J. Savage, *Phys. Rev. Lett.* **97**, 012001 (2006), hep-lat/0602010.
- [11] S. R. Beane, P. F. Bedaque, T. C. Luu, K. Orginos, E. Pallante, A. Parreno, and M. J. Savage (NPLQCD), *Nucl. Phys. A* **794**, 62 (2007), hep-lat/0612026.
- [12] S. R. Beane et al. (NPLQCD), *Phys. Rev. Lett.* **106**, 162001 (2011), 1012.3812.
- [13] S. R. Beane et al., *Mod. Phys. Lett. A* **26**, 2587 (2011), 1103.2821.
- [14] S. R. Beane, E. Chang, W. Detmold, H. W. Lin, T. C. Luu, K. Orginos, A. Parreno, M. J. Savage, A. Torok, and A. Walker-Loud (NPLQCD), *Phys. Rev. D* **85**, 054511 (2012), 1109.2889.
- [15] S. R. Beane, E. Chang, S. D. Cohen, W. Detmold, H. W. Lin, T. C. Luu, K. Orginos, A. Parreno, M. J. Savage, and A. Walker-Loud (NPLQCD), *Phys. Rev. D* **87**, 034506 (2013), 1206.5219.
- [16] K. Orginos, A. Parreno, M. J. Savage, S. R. Beane, E. Chang, and W. Detmold, *Phys. Rev. D* **92**, 114512 (2015), [Erratum: *Phys.Rev.D* 102, 039903 (2020)], 1508.07583.
- [17] M. L. Wagman, F. Winter, E. Chang, Z. Davoudi, W. Detmold, K. Orginos, M. J. Savage, and P. E. Shanahan, *Phys. Rev. D* **96**, 114510 (2017), 1706.06550.
- [18] M. Fukugita, Y. Kuramashi, M. Okawa, H. Mino, and A. Ukawa, *Phys. Rev. D* **52**, 3003 (1995), hep-lat/9501024.
- [19] T. Yamazaki, Y. Kuramashi, and A. Ukawa (PACS-CS), *Phys. Rev. D* **84**, 054506 (2011), 1105.1418.
- [20] T. Yamazaki, K.-i. Ishikawa, Y. Kuramashi, and A. Ukawa, *Phys. Rev. D* **86**, 074514 (2012), 1207.4277.
- [21] T. Yamazaki, K.-i. Ishikawa, Y. Kuramashi, and A. Ukawa, *Phys. Rev. D* **92**, 014501 (2015), 1502.04182.
- [22] H. Nemura, N. Ishii, S. Aoki, and T. Hatsuda, *Phys. Lett. B* **673**, 136 (2009), 0806.1094.
- [23] T. Inoue (HAL QCD), *AIP Conf. Proc.* **1441**, 335 (2012), 1109.1620.
- [24] E. Berkowitz, T. Kurth, A. Nicholson, B. Joo, E. Rinaldi, M. Strother, P. M. Vranas, and A. Walker-Loud, *Phys. Lett. B* **765**, 285 (2017), 1508.00886.
- [25] A. Francis, J. R. Green, P. M. Junnarkar, C. Miao, T. D. Rae, and H. Wittig, *Phys. Rev. D* **99**, 074505 (2019), 1805.03966.
- [26] P. Junnarkar and N. Mathur, *Phys. Rev. Lett.* **123**, 162003 (2019), 1906.06054.
- [27] B. Hörz et al., *Phys. Rev. C* **103**, 014003 (2021), 2009.11825.
- [28] M. Illa et al. (NPLQCD), *Phys. Rev. D* **103**, 054508 (2021), 2009.12357.
- [29] J. R. Green, A. D. Hanlon, P. M. Junnarkar, and H. Wittig, *Phys. Rev. Lett.* **127**, 242003 (2021), 2103.01054.
- [30] T. Iritani et al. (HAL QCD), *Phys. Lett. B* **792**, 284 (2019), 1810.03416.
- [31] K. Murakami, Y. Akahoshi, S. Aoki, T. Doi, and K. Sasaki (Sasaki(HAL QCD)Collaboration), *Kenji*, *PTEP* **2023**, 043B05 (2023), 2210.05395.
- [32] V. Braun and D. Müller, *Eur. Phys. J. C* **55**, 349 (2008), 0709.1348.
- [33] X. Ji, *Phys. Rev. Lett.* **110**, 262002 (2013), 1305.1539.
- [34] X. Ji, *Sci. China Phys. Mech. Astron.* **57**, 1407 (2014), 1404.6680.
- [35] Y.-Q. Ma and J.-W. Qiu, *Phys. Rev. Lett.* **120**, 022003 (2018), 1709.03018.
- [36] H.-W. Lin et al., *Prog. Part. Nucl. Phys.* **100**, 107 (2018), 1711.07916.
- [37] A. V. Radyushkin, *Phys. Rev. D* **96**, 034025 (2017), 1705.01488.
- [38] Y.-S. Liu et al. (Lattice Parton), *Phys. Rev. D* **101**, 034020 (2020), 1807.06566.
- [39] J.-W. Chen, L. Jin, H.-W. Lin, Y.-S. Liu, Y.-B. Yang, J.-H. Zhang, and Y. Zhao (2018), 1803.04393.
- [40] H.-W. Lin, J.-W. Chen, X. Ji, L. Jin, R. Li, Y.-S. Liu, Y.-B. Yang, J.-H. Zhang, and Y. Zhao, *Phys. Rev. Lett.* **121**, 242003 (2018), 1807.07431.
- [41] H.-W. Lin, J.-W. Chen, T. Ishikawa, and J.-H. Zhang (LP3), *Phys. Rev. D* **98**, 054504 (2018), 1708.05301.
- [42] Y.-S. Liu, J.-W. Chen, L. Jin, R. Li, H.-W. Lin, Y.-B. Yang, J.-H. Zhang, and Y. Zhao (2018), 1810.05043.
- [43] F. Yao et al. (Lattice Parton), *Phys. Rev. Lett.* **131**, 261901 (2023), 2208.08008.
- [44] K. Orginos, A. Radyushkin, J. Karpie, and S. Zafeiropoulos, *Phys. Rev. D* **96**, 094503 (2017), 1706.05373.
- [45] C. Alexandrou, K. Cichy, V. Drach, E. Garcia-Ramos, K. Hadjiyiannakou, K. Jansen, F. Steffens, and C. Wiese, *Phys. Rev. D* **92**, 014502 (2015), 1504.07455.
- [46] C. Alexandrou, K. Cichy, M. Constantinou, K. Hadjiyiannakou, K. Jansen, A. Scapellato, and F. Steffens, *Phys. Rev. Lett.* **125**, 262001 (2020), 2008.10573.
- [47] X. Gao, A. D. Hanlon, J. Holligan, N. Karthik, S. Mukherjee, P. Petreczky, S. Syritsyn, and Y. Zhao, *Phys. Rev. D* **107**, 074509 (2023), 2212.12569.

- [48] J. Karpie, K. Orginos, A. Radyushkin, and S. Zafeiropoulos (HadStruc), *JHEP* **11**, 024 (2021), 2105.13313.
- [49] R. G. Edwards et al. (HadStruc), *JHEP* **03**, 086 (2023), 2211.04434.
- [50] X. Ji, Y.-S. Liu, Y. Liu, J.-H. Zhang, and Y. Zhao, *Rev. Mod. Phys.* **93**, 035005 (2021), 2004.03543.
- [51] X. Ji, Y. Liu, A. Schäfer, W. Wang, Y.-B. Yang, J.-H. Zhang, and Y. Zhao, *Nucl. Phys. B* **964**, 115311 (2021), 2008.03886.
- [52] J. Hua et al. (Lattice Parton), *Phys. Rev. Lett.* **129**, 132001 (2022), 2201.09173.
- [53] J. Hua, M.-H. Chu, P. Sun, W. Wang, J. Xu, Y.-B. Yang, J.-H. Zhang, and Q.-A. Zhang (Lattice Parton), *Phys. Rev. Lett.* **127**, 062002 (2021), 2011.09788.
- [54] Z.-C. Hu, B.-L. Hu, J.-H. Wang, M. Gong, L. Liu, P. Sun, W. Sun, W. Wang, Y.-B. Yang, and D.-J. Zhao (2023), 2310.00814.
- [55] H.-Y. Du et al. (2024), 2408.03548.
- [56] M. Constantinou and H. Panagopoulos, *Phys. Rev. D* **96**, 054506 (2017), 1705.11193.
- [57] J. Green, K. Jansen, and F. Steffens, *Phys. Rev. Lett.* **121**, 022004 (2018), 1707.07152.
- [58] J.-W. Chen, T. Ishikawa, L. Jin, H.-W. Lin, J.-H. Zhang, and Y. Zhao (LP3), *Chin. Phys. C* **43**, 103101 (2019), 1710.01089.
- [59] C. Alexandrou, M. Constantinou, K. Hadjiyiannakou, K. Jansen, and F. Manigrasso, *Phys. Rev. D* **104**, 054503 (2021), 2106.16065.
- [60] G. S. Bali, B. Lang, B. U. Musch, and A. Schäfer, *Phys. Rev. D* **93**, 094515 (2016), 1602.05525.
- [61] J.-W. Chen, X. Ji, and J.-H. Zhang, *Nucl. Phys. B* **915**, 1 (2017), 1609.08102.
- [62] T. Izubuchi, X. Ji, L. Jin, I. W. Stewart, and Y. Zhao, *Phys. Rev. D* **98**, 056004 (2018), 1801.03917.
- [63] C. Alexandrou, K. Cichy, M. Constantinou, K. Hadjiyiannakou, K. Jansen, H. Panagopoulos, and F. Steffens, *Nucl. Phys. B* **923**, 394 (2017), 1706.00265.
- [64] A. Radyushkin, *Phys. Rev. D* **98**, 014019 (2018), 1801.02427.
- [65] V. M. Braun, A. Vladimirov, and J.-H. Zhang, *Phys. Rev. D* **99**, 014013 (2019), 1810.00048.
- [66] Z.-Y. Li, Y.-Q. Ma, and J.-W. Qiu, *Phys. Rev. Lett.* **122**, 062002 (2019), 1809.01836.
- [67] Y.-K. Huo et al. (Lattice Parton Collaboration (LPC)), *Nucl. Phys. B* **969**, 115443 (2021), 2103.02965.
- [68] C.-Y. Chou and J.-W. Chen, *Phys. Rev. D* **106**, 014507 (2022), 2204.08343.
- [69] F. Yao, Y. Ji, and J.-H. Zhang, *JHEP* **11**, 021 (2023), 2212.14415.
- [70] R. Zhang, J. Holligan, X. Ji, and Y. Su, *Phys. Lett. B* **844**, 138081 (2023), 2305.05212.
- [71] Y. Su, J. Holligan, X. Ji, F. Yao, J.-H. Zhang, and R. Zhang, *Nucl. Phys. B* **991**, 116201 (2023), 2209.01236.
- [72] R. G. Edwards and B. Joo (SciDAC, LHPC, UKQCD), *Nucl. Phys. B Proc. Suppl.* **140**, 832 (2005), hep-lat/0409003.
- [73] M. A. Clark, R. Babich, K. Barros, R. C. Brower, and C. Rebbi (QUDA), *Comput. Phys. Commun.* **181**, 1517 (2010), 0911.3191.
- [74] R. Babich, M. A. Clark, B. Joo, G. Shi, R. C. Brower, and S. Gottlieb (QUDA), in *International Conference for High Performance Computing, Networking, Storage and Analysis* (2011), 1109.2935.
- [75] M. A. Clark, B. Joó, A. Strelchenko, M. Cheng, A. Gambhir, and R. C. Brower (QUDA), in *International Conference for High Performance Computing, Networking, Storage and Analysis* (2016), 1612.07873.
- [76] Y.-J. Bi, Y. Xiao, W.-Y. Guo, M. Gong, P. Sun, S. Xu, and Y.-B. Yang, *PoS LATTICE2019*, 286 (2020), 2001.05706.
- [77] G. S. Bali, C. Bauer, A. Pineda, and C. Torrero, *Phys. Rev. D* **87**, 094517 (2013), 1303.3279.